Optical Society of America. Hwi Kim, Sung-Wook Min, Byoungho Lee, and Ting-Chung Poon, "Optical sectioning for optical scanning holography using phase-space filtering with Wigner distribution functions," Appl. Opt. 47, D164-D175 (2008). doi: 10.1364/ao.47.00d164

Optical sectioning for optical scanning holography using phase-space filtering with Wigner distribution functions

Hwi Kim,[1] Sung-Wook Min,[2,*] Byoungho Lee,[1] and Ting-Chung Poon[3]

[1]National Creative Research Center for Active Plasmonics Applications Systems, School of Electrical Engineering, Seoul National University, Kwanak-Gu Shinlim-Dong, Seoul 151-744, South Korea

[2]Department of Information Display, College of Science, Kyung Hee University, Hoeki-dong, Dongdaemoon-ku Seoul 130-701, South Korea

[3]Bradley Department of Electrical and Computer Engineering, Virginia Polytechnic Institute and State University, Blacksburg, Virginia 24061, USA

*Corresponding author: mins@khu.ac.kr

Received 15 October 2007; revised 4 February 2008; accepted 13 March 2008; posted 14 March 2008 (Doc. ID 88657); published 22 April 2008

We propose a novel optical sectioning method for optical scanning holography, which is performed in phase space by using Wigner distribution functions together with the fractional Fourier transform. The principle of phase-space optical sectioning for one-dimensional signals, such as slit objects, and two-dimensional signals, such as rectangular objects, is first discussed. Computer simulation results are then presented to substantiate the proposed idea. © 2008 Optical Society of America

OCIS codes: 090.1760, 180.6900, 070.2580, 100.3010.

1. Introduction

Optical sectioning is considered to be one of the most important topics for three-dimensional (3-D) imaging in microscopy. High-numerical-aperture objective lenses are required for high-resolution spatial analysis, but they have a very limited depth of focus. Hence it is difficult to image an entire 3-D cell clearly. Any image of the specimen is contaminated with out-of-focus information from focal planes above and below the current focus setting [1–3]. Castleman [4] and Agard [3] proposed the use of nearest-neighbor planes, i.e., a plane above and a plane below the focal plane, to remove the out-of-focus noise from the focal plane in 3-D microscopy. Recently, optical sectioning in holography was investigated by Leith *et al.* [5], and Wiener filtering was proposed by Kim [6] to reduce the defocus noise in the reconstruction of a 3-D image from a complex hologram obtained by optical scanning holography (OSH). In this paper, we propose a novel optical sectioning method for complex holograms recorded by OSH. The hologram is processed by phase-space filtering using a Wigner distribution function (WDF) together with the notion of the fractional Fourier transform (FRFT). Using the WDF, we show that on a given focused plane the focused information and the defocused information are separated in the phase space, and hence a filter in the phase space can be designed to block the defocused information. We show simulation results for slit objects and rectangular objects to verify our idea.

In Section 2, we briefly review OSH, WDF, and FRFT. In Section 3, we propose the idea of optical sectioning using the WDF and FRFT, and computer simulation results for one-dimensional (1-D) signals are presented to substantiate the proposed idea. In Section 4, optical sectioning using WDF is applied to two-dimensional (2-D) images. Finally, in Section 5, we make some concluding remarks.

0003-6935/08/19D164-12$15.00/0

2. Optical Scanning Holography, Optical Sectioning, Wigner Distribution, and Fractional Fourier Transform

A. Optical Scanning Holography and Optical Sectioning

Optical sectioning in holography has been investigated [5], and most recently Wiener filtering has been proposed to reduce the defocus noise in the reconstruction of a 3-D image from a complex hologram obtained by OSH [6]. OSH is a recording technique that can record 3-D holographic information by using a single 2-D optical heterodyne scan [7]. It has been applied to many applications, such as 3-D microscopy [8] and 3-D pattern recognition [9]. In this work, we investigate a novel optical sectioning technique for OSH.

In OSH, a complex Fresnel zone plate hologram is generated and is given by [10]

$$\varphi(x,y) = \int |O(x,y;z)|^2 \otimes \frac{k_o}{2\pi z}\exp[-\frac{jk_0}{2z}(x^2+y^2)]\mathrm{d}z, \tag{1}$$

where the 3-D object is modeled as a collection of planar intensity distributions, $|O(x,y;z)|^2$, and z is the thickness parameter of the object. $\otimes$ is the 2-D convolution operation involving x and y [11]. It is important to point out that the complex hologram contains no twin-image information; i.e., upon reconstruction of the complex hologram, twin-image noise does not appear. If $|O(x,y;z)|^2 = I(x,y)\delta(z-z_0)$, a planar intensity distribution located along z_0, then the complex hologram, according to Eq. (1), is

$$\varphi(x,y) = I(x,y) \otimes \frac{k_o}{2\pi z_0}\exp\left[-\frac{jk_0}{2z_0}(x^2+y^2)\right]. \tag{2}$$

To reconstruct the hologram, we can illuminate it with a plane wave to give a diffraction pattern at z away from the hologram as

$$\varphi(x,y) \otimes h(x,y,z) = I(x,y) \otimes \frac{k_o}{2\pi z_0}\exp\left[-\frac{jk_0}{2z_0}(x^2+y^2)\right] \otimes h(x,y;z), \tag{3}$$

where

$$h(x,y,z) = -\frac{jk_o}{2\pi z}\exp\left[\frac{jk_0}{2z}(x^2+y^2)\right] \tag{4}$$

is the free-space spatial impulse response in Fourier optics if we neglect a constant phase factor [11]. A real image is formed z_0 away from the hologram as, from Eq. (3), we let $z = z_0$ to give

$$\begin{aligned}\varphi(x,y) \otimes h(x,y,z_0) &= I(x,y) \otimes \frac{k_o}{2\pi z_0}\exp\left[-\frac{jk_0}{2z_0}(x^2+y^2)\right] \otimes h(x,y;z_0)\\ &\propto I(x,y) \otimes \delta(x,y) = I(x,y).\end{aligned} \tag{5}$$

Note that there is no twin image on the real image plane.

Now, for a 3-D object, if the complex hologram is illuminated by a plane wave, the sectional image at a certain depth, say, at z_R is given by

$$\begin{aligned}s_{z_R} &= \varphi(x,y) \otimes h(x,y;z_R)\\ &= |O(x,y;z_R)|^2 + \int_{z\neq z_R} |O(x,y;z)|^2 \otimes h(x,y;z-z_R)\mathrm{d}z = f(x,y;z_R) + \int_{z\neq z_R} f(x,y;z) \otimes h(x,y;z-z_R)\mathrm{d}z,\end{aligned} \tag{6}$$

where $f(x,y,z_R)$ is the sectional image at $z = z_R$. $\int_{z\neq z_R} f(x,y;z) \otimes h(x,y;z-z_R)\mathrm{d}z$ is the term of defocus noise on the $z = z_R$ plane to be filtered or rejected. The idea of optical sectioning is to reject or filter this term while keeping the integrity of the sectional focused image $f(x,y,z_R)$.

B. Wigner Distribution Function and the Fractional Fourier Transform

The phase-space representation of optical fields often provides a very powerful analysis tool for optical signal processing [12–14]. In particular, signal filtering benefits from the phase-space representation of optical signals. The central part of the phase space filtering of optical signals is the WDF. The WDF $W_f(x_1,x_2,\mu_1,\mu_2)$ of a 2-D complex signal $f(x_1,x_2)$ is defined by

$$\begin{aligned}W_f(x_1,x_2,\mu_1,\mu_2) = \iint & f(x_1 + x_1'/2, x_2 + x_2'/2) f^*(x_1 - x_1'/2, x_2 - x_2'/2) e^{-j2\pi(\mu_1 x_1' + \mu_2 x_2')}\mathrm{d}x_1'\mathrm{d}x_2'.\end{aligned} \tag{7}$$

The WDF is a 4-D distribution function for 2-D optical signals. The complex signal $f(x_1,x_2)$ can be reconstructed by the following reconstruction formula:

$$f(x_1,x_2) = \frac{1}{f^*(x_{m,1},x_{m,2})} \times \iint W_f\left(\frac{x_1+x_{m,1}}{2}, \frac{x_2+x_{m,2}}{2}, \mu_1, \mu_2\right) \times e^{j2\pi(\mu_1(x_1-x_{m,1})+\mu_2(x_2-x_{m,2}))}\mathrm{d}\mu_1\mathrm{d}\mu_2. \tag{8}$$

The signal reconstruction takes the form of the inverse Fourier transform of the WDF. The WDF has an interesting geometric property for the FRFT of a signal.

The ath-order 2-D FRFT of f, $Frt^{(a)}\{f\}$, is defined by [13,15]

$$Frt^{(a)}\{f(x_1',x_2')\} = f_a(x_1,x_2) = \int_{-\infty}^{\infty} K_a(x_1,x_1')K_a(x_2,x_2')f(x_1',x_2')\mathrm{d}x_1'\mathrm{d}x_2', \tag{9}$$

where the integral kernel $K_a(x,x')$ is defined by

$$K_a(x,x') = \begin{cases} \sqrt{1-j\times\ \cot\chi}\exp(j\pi[\cot\chi x^2 - 2\csc\chi xx' + \cot\chi x'^2]) & \text{for } \chi \neq \pi m \\ \delta(x-x') & \text{for } \chi = 2\pi m \\ \delta(x+x') & \text{for } \chi = 2\pi m \pm \pi \end{cases}, \tag{10}$$

and where χ is the angular expression of the FRFT order a defined by $\chi = \pi a/2$. The WDF of $f_a(x_1,y_1)$ is given by

$$\begin{aligned} W_{f_a}(x_1,\mu_1,x_2,\mu_2) = W_{f_a}(&x_1\cos\chi - \mu_1\sin\chi, x_1\sin\chi \\ &+ \mu_1\cos\chi, x_2\cos\chi \\ &- \mu_2\sin\chi, x_2\sin\chi + \mu_2\cos\chi). \end{aligned} \tag{11}$$

The WDF of $f_a(x_1,y_1)$ is equal to the distribution geometrically rotated by an angle χ. This feature of the WDF can be exploited for various signal processing or filtering applications [13].

In general, paraxial optical systems can be equivalently described with a well-defined FRFT with specific FRFT order and proper scaling factors. In [15], the linear integral transformation of a paraxial optical system is represented by the ath-order 2-D FRFT in the form

$$f_a(x_1,x_2) = \int_{-\infty}^{\infty}\int_{-\infty}^{\infty} h^{(a)}(x_1,x_2,x_1',x_2')f(x_1',x_2')\mathrm{d}x_1'\mathrm{d}x_2', \tag{12}$$

where the transform kernel is given by

$$\begin{aligned} h^{(a)}(x_1,x_2,x_1',x_2') = &\frac{\csc(\chi)}{s^2}e^{-j\pi/2} \\ &\times\exp(j\frac{\pi}{s^2}[\cot(\chi)(x^2+y^2) \\ &- 2\csc(\chi)(xx'+yy') \\ &+ \cot(\chi)(x'^2+y'^2)]). \end{aligned} \tag{13}$$

The above kernel maps a function $f(x_1',x_2') = (1/s)\hat{f}(x_1'/s,x_2'/s)$ into $(1/s)\hat{f}_a(x_1/s,x_2/s)$, where s is a scaling factor and $\hat{f}_a(x_1,x_2)$ is the ath-order 2-D FRFT of $\hat{f}(x_1,x_2)$.

Here, for convenience, we assume that the holographic real image reconstruction of OSH is to be represented by a single focusing lens. The situation is shown in Fig. 1. In Fig. 1, the positions at $z = z_1$ and $z = z_2$ indicate two sectional image planes.

We assume that the 3-D intensity distribution of a 3-D object, $|O(x,y;z)|^2$, takes the form

$$\begin{aligned} |O(x,y;z)|^2 = &f_1(x_1,x_2,z_1)\delta(z-z_1) \\ &+ f_2(x_1,x_2,z_2)\delta(z-z_2), \end{aligned} \tag{14}$$

where $f_1(x_1,x_2,z_1)$ and $f_2(x_1,x_2,z_2)$ are the two sectional images.

By substituting Eq. (14) into Eq. (1), we can model the complex hologram in OSH by

$$\begin{aligned} \varphi(x_1,x_2) = &f_1(x_1,x_2,z_1)\oplus h^{(a_1)}(x_1,x_2,z_1) \\ &+ f_2(x_1,x_2,z_2)\oplus h^{(a_2)}(x_1,x_2,z_2), \end{aligned} \tag{15}$$

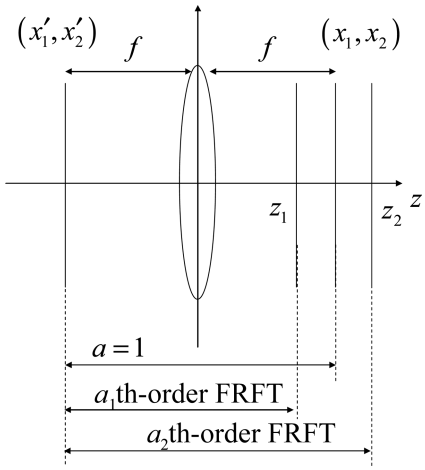

Fig. 1. Single-lens optical system representing holographic reconstruction of real images by a complex hologram obtained by OSH. Note that the defocused planes are modeled by the FFRT, whereas the in-focus plane is represented by a pure Fourier transform.

where $\oplus$ denotes the integral transform operation given by Eq. (12), and we have replaced the convolution operation in Eq. (1) by the general linear canonical transform [13].

Similarly, from Eq. (6), the reconstruction process of the signals $s_{z_1}(x_1,x_2)$ and $s_{z_2}(x_1,x_2)$ can be stated, respectively, as

$$\begin{aligned} s_{z_1}(x_1,x_2) &= \varphi(x_1,x_2)\oplus h^{(a_1)*}(x_1,x_2) \\ &= \varphi(x_1,x_2)\oplus h^{(-a_1)}(x_1,x_2) \\ &= f_1(x_1,x_2,z_1)\oplus h^{(a_1)}(x_1,x_2) \\ &\quad \oplus h^{(-a_1)}(x_1,x_2) \\ &\quad + f_2(x_1,x_2,z_2)\oplus h^{(a_2)}(x_1,x_2) \\ &\quad \oplus h^{(-a_1)}(x_1,x_2) \\ &= f_1(x_1,x_2,z_1) + f_2(x_1,x_2,z_2) \\ &\quad \oplus h^{(a_2-a_1)}(x_1,x_2), \end{aligned} \tag{16a}$$

$$\begin{aligned} s_{z_2}(x,y) &= \varphi(x,y)\oplus h^{(a_2)*}(x,y) \\ &= \varphi(x,y)\oplus h^{(-a_2)}(x,y) \\ &= f_1(x,y,z_1)\oplus h^{(a_1)}(x,y) \\ &\quad \oplus h^{(-a_2)}(x,y) \\ &\quad + f_2(x,y,z_2)\oplus h^{(a_2)}(x,y) \\ &\quad \oplus h^{(-a_2)}(x,y) \\ &= f_1(x,y,z_1)\oplus h^{(a_1-a_2)}(x,y) \\ &\quad + f_2(x,y,z_2). \end{aligned} \tag{16b}$$

Let us demonstrate the relationship between the FRFT order and the geometry of the single optical system shown in Fig. 1. From [16,17], we can see that the mathematical representation of the optical transform of the simple focusing lens shown in Fig. 1 is given by

$$\begin{aligned} h(x_1,x_2,x_1',x_2') = \frac{-j}{\lambda f}\exp\left(\frac{j\pi}{\lambda f}\left[-2(x_1x_1'+x_2x_2')\right.\right. \\ \left.\left.+\left(1-\frac{d}{f}\right)(x_1'^2+x_2'^2)\right]\right), \end{aligned} \tag{17}$$

where f is the focal length of the lens.

If we use proper parameters and neglect the spherical phase profile in the fractional domain (x_1,x_2), the transform kernel in Eq. (13) becomes Eq. (17) [see [15], also]. Let z_1 and z_2 in Fig. 1 be given, respectively, by the symmetric values

$$z_1 = f - \Delta z, \tag{18a}$$

$$z_2 = f + \Delta z. \tag{18b}$$

By comparing Eq. (13) with Eq. (17), we can obtain the relationship between the FRFT order and the geometric factors of the focusing lens as

$$a_1 = \frac{2}{\pi}\cos^{-1}\left(\frac{\Delta z}{f}\right), \tag{19a}$$

$$a_2 = \frac{2}{\pi}\cos^{-1}\left(-\frac{\Delta z}{f}\right) = 2 - a_1, \tag{19b}$$

where a_1 and a_2 correspond to the situation of imaging planes at z_1 and z_2, respectively.

The two sectional images placed on the symmetric sectional planes are included in the simulation examples, for convenience. Hence, using Eqs. (19a) and (19b), the reconstructed signals $f_1(x,y,z_1)$ and $f_2(x,y,z_2)$ from Eqs. (16a) and (16b) are obtained, respectively, by

$$\begin{aligned} s_{z_1}(x_1,x_2) &= f_1(x_1,x_2,z_1) \\ &\quad + f_2(x_1,x_2,z_2)\oplus h^{(2-2a_1)}(x_1,x_2), \end{aligned} \tag{20a}$$

$$\begin{aligned} s_{z_2}(x_1,x_2) &= f_1(x_1,x_2,z_1)\oplus h^{(2a_1-2)}(x_1,x_2) \\ &\quad + f_2(x_1,x_2,z_2). \end{aligned} \tag{20b}$$

3. Optical Sectioning of One-Dimensional Signals

In this section, the basic principle of the proposed phase-space optical sectioning is elucidated by the investigation of optical sectioning of two slit objects displaced along the depth direction. From Eq. (7), the 1-D version of the WDF and the reconstruction formula are given, respectively, by

$$W_f(x,\mu) = \int f(x+x'/2)f^*(x-x'/2)e^{-j2\pi\mu x'}\mathrm{d}x', \tag{21a}$$

$$f(x) = \frac{1}{f^*(x_m)}\int_{-\infty}^{\infty} W\left(\frac{x+x_m}{2},\mu\right)e^{i2\pi\mu(x+x_m)}\mathrm{d}\mu. \tag{21b}$$

The WDF of the ath-order FRFT of $f(x)$ is similarly given by

$$\begin{aligned} &W_{f_a}(x,\mu) \\ &\quad = W_{f_a}(x\cos\chi - \mu\sin\chi, x\sin\chi + \mu\cos\chi). \end{aligned} \tag{22}$$

Let us consider two slit objects, $f_1(x)$ and $f_2(x)$. Figure 2 illustrates examples of sectional signals $f_1(x)$ and $f_2(x)$ and the evolutionary profiles of their FRFTs with the FRFT order increased from 0 to 1. $f_1(x)$ is a rectangular function (slit pattern), the

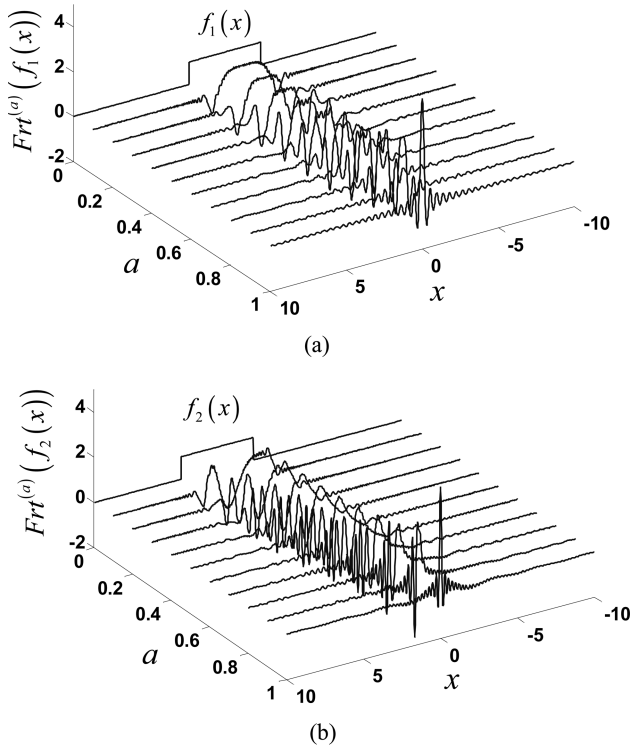

Fig. 2. Evolutionary profiles of FRFTs of example sectional signals (a) $f_1(x)$ and (b) $f_2(x)$.

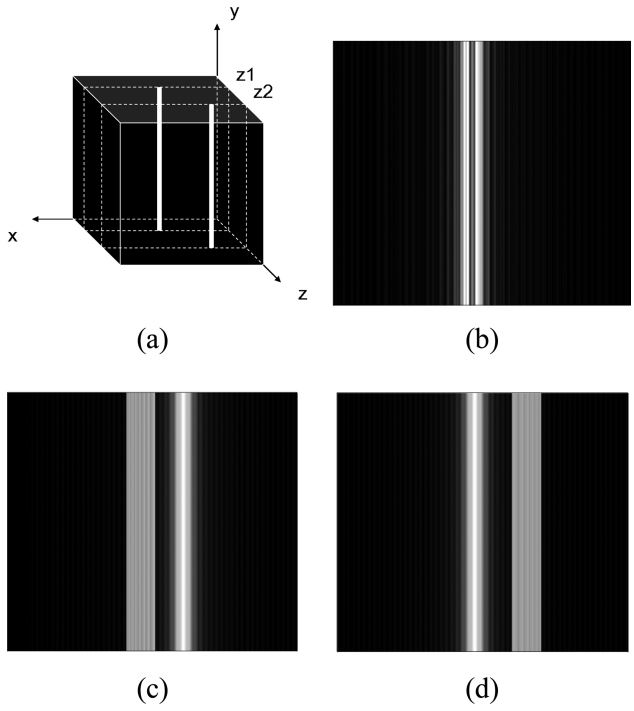

Fig. 3. (a) Two slits, (b) amplitude profile of the complex hologram $\varphi(x)$ given by Eq. (23), (c) $s_{z_1}(x)$ given by Eq. (24a), (d) $s_{z_2}(x)$ given by Eq. (24b).

center of which is placed at $x = 0$, while $f_2(x)$ is also a rectangular function with the center at $x = 2$.

Let us simulate the complex hologram and image reconstruction without and with the optical sectioning process proposed in the paper. To clearly prove the main idea, we also present the optical sectioning of two comparable cases of two-slit objects without and with spatial overlapping.

A. Optical Sectioning of Two-Slit Object without Spatial Overlapping

Figure 3(a) shows sectional signals $f_1(x)$ and $f_2(x)$ and their relative positions in a 3-D Cartesian coordinate system. In this example, spatial overlapping does not exist between $f_1(x)$ and $f_2(x)$. Employing the focusing lens as shown in Fig. 1 to represent real image reconstruction in OSH, let us assume that the complex hologram takes the form of Eq. (15):

$$\varphi(x) = f_1(x, z_1) \oplus h^{(3/4)}(x) + f_2(x, z_2) \oplus h^{(5/4)}(x), \quad (23)$$

where the FRFT orders of the signals $f_1(x)$ and $f_2(x)$ that are recorded as a hologram are taken as $3/4$ and $5/4$, respectively, for simulation purposes. Note that the FRFT orders are chosen according to the criterion established in Eq. (19b). In Fig. 3(b), the amplitude profile of the synthesized OSH complex hologram is presented.

Within this setup, the reconstructed sectional signals without optical sectioning processing are given by, from Eqs. (19a), (19b), (20a), and (20b),

$$\begin{aligned} s_{z_1}(x) &= f_1(x, z_1) + f_2(x, z_2) \oplus h^{(0.5)}(x) \\ &= f_1(x, z_1) + f_{2,0.5}(x, z_2), \end{aligned} \quad (24a)$$

$$\begin{aligned} s_{z_2}(x) &= f_1(x, z_1) \oplus h^{(-0.5)}(x) + f_2(x, z_2) \\ &= f_{1,-0.5}(x, z_1) + f_2(x, z_2). \end{aligned} \quad (24b)$$

The reconstructed sectional signals $s_{z_1}(x)$ and $s_{z_2}(x)$ are shown in Figs. 3(c) and 3(d), respectively. As is seen in Figs. 3(c) and 3(d), the reconstructed signals include both the focused signal and the defocused signal. In Fig. 3(c), the left-hand slit is in focus, whereas the right-hand slit is defocused. In Fig. 3(d), the right-hand slit is in focus and the left-hand slit is out of focus.

Optical sectioning refers to blocking out or rejecting defocused signals from reaching the focused reconstruction sectional plane. We devise an optical sectioning method using the filtering of the WDF of the reconstructed signal contaminated by defocused signals. First, let us calculate the WDFs of $s_{z_1}(x)$ and $s_{z_2}(x)$. Using Eqs. (7), (24a),

and (24b), the WDFs of $s_{z_1}(x)$ and $s_{z_2}(x)$ are derived, respectively, as

$$\begin{aligned} W_{f_1+f_{2,a}}(x,\mu) &= \int [f_1(x+x'/2) \\ &\quad + f_{2,a}(x+x'/2)][f_1^*(x-x'/2) \\ &\quad + f_{2,a}^*(x-x'/2)]e^{-j2\pi\mu x'}\,\mathrm{d}x' \\ &= W_{f_1}(x,\mu) + W_{f_{2,a}}(x,\mu) \\ &\quad + 2\,\mathrm{Re}\left\{e^{j4\pi\mu x}\int f_{2,a}\left(\frac{x''}{2}\right)\right. \\ &\quad \left.\times f_1^*\left(2x-\frac{x''}{2}\right)e^{-j2\pi\mu x''}\,\mathrm{d}x''\right\} \\ &= W_{f_1}(x,\mu) + W_{f_{2,a}}(x,\mu) \\ &\quad + C_{f_1+f_{2,a}}(x,\mu), \end{aligned} \tag{25a}$$

$$\begin{aligned} W_{f_{1,-a}+f_2}(x,\mu) &= \int [f_{1,-a}(x+x'/2) \\ &\quad + f_2(x+x'/2)][f_{1,-a}^*(x-x'/2) \\ &\quad + f_2^*(x-x'/2)]e^{-j2\pi\mu x'}\,\mathrm{d}x' \\ &= W_{f_{1,-a}}(x,\mu) + W_{f_2}(x,\mu) \\ &\quad + 2\,\mathrm{Re}\left\{e^{j4\pi\mu x}\int f_{1,-a}\left(\frac{x''}{2}\right)\right. \\ &\quad \left.\times f_2^*\left(2x-\frac{x''}{2}\right)e^{-j2\pi\mu x''}\,\mathrm{d}x''\right\} \\ &= W_{f_{1,-a}}(x,\mu) + W_{f_2}(x,\mu) \\ &\quad + C_{f_{1,-a}+f_2}(x,\mu). \end{aligned} \tag{25b}$$

In our simulations, a in Eqs. (25a) and (25b) is given by 0.5 as suggested by Eqs. (24a) and (24b). From the above results, we can identify that the WDF is composed of three terms: the WDF of the focused signal, the WDF of the defocused signal, and the cross term. The results of $W_{f_1+f_{2,a}}(x,\mu)$ and $W_{f_{1,-a}+f_2}(x,\mu)$ are illustrated, respectively, in Figs. 4(a) and 5(a) for $a = 0.5$. The three partial terms comprising the WDF are separately shown in Figs. 4 and 5 to aid understanding of the filtering principle.

Filtering in the phase-space domain is performed to eliminate the parts of the defocused signal and the cross term. We simply use a binary filter to perform filtering. The most useful property of the WDF in phase space is that the defocused signal is separated by the geometric rotation. In this example, we can effectively remove the cross term from the WDF in phase space as seen in Figs. 4 and 5 by a binary filter in the phase-space domain. A sectional image is reconstructed from the filtered WDF.

In Figs. 6 and 7, the WDF filtering and signal reconstruction of $f_1(x)$ from $s_{z_1}(x)$ and those of $f_1(x)$ from $s_{z_1}(x)$ are illustrated, respectively. The filtered

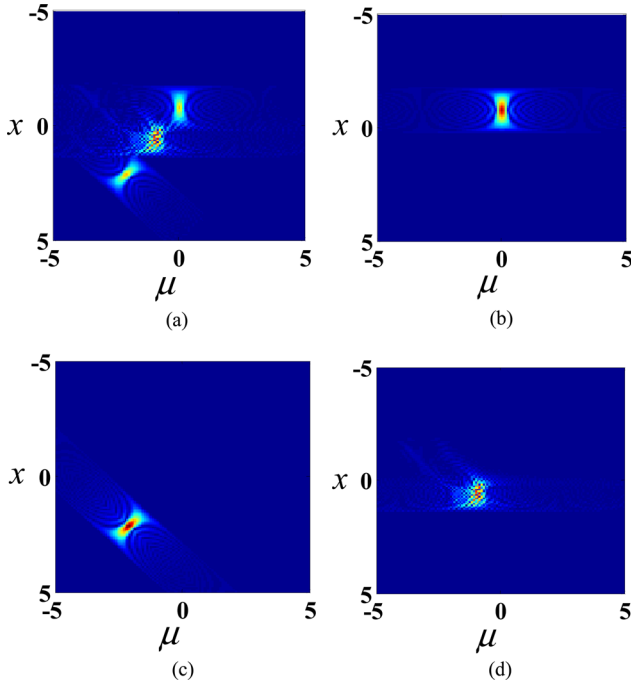

Fig. 4. (Color online) (a) WDF of $s_{z_1}(x)$: $W_{f_1+f_{2,a}}(x,\mu)$, (b) $W_{f_1}(x,\mu)$, (c) $W_{f_{2,a}}(x,\mu)$, (d) $C_{f_1+f_{2,a}}(x,\mu)$.

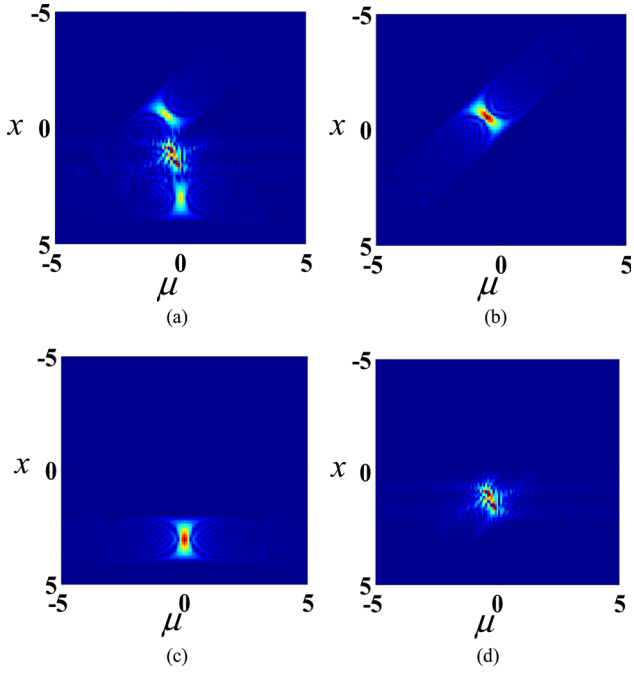

Fig. 5. (Color online) (a) WDF of $s_{z_2}(x)$: $W_{f_{1,-a}+f_2}(x,\mu)$, (b) $W_{f_{1,-a}}(x,\mu)$, (c) $W_{f_2}(x,\mu)$, (d) $C_{f_{1,-a}+f_2}(x,\mu)$.

WDF, W_1, of $W_{f_1+f_{2,a}}(x,\mu)$ obtained by a binary filter is shown in Fig. 6(a). In Figs. 6(b) and 6(c), the unfiltered reconstructed signal $s_{z_1}(x)$ and the filtered reconstructed signal $\bar{f}_1(x)$ are presented, respectively. Clearly, in Fig. 6(c), we observe that the slit on the

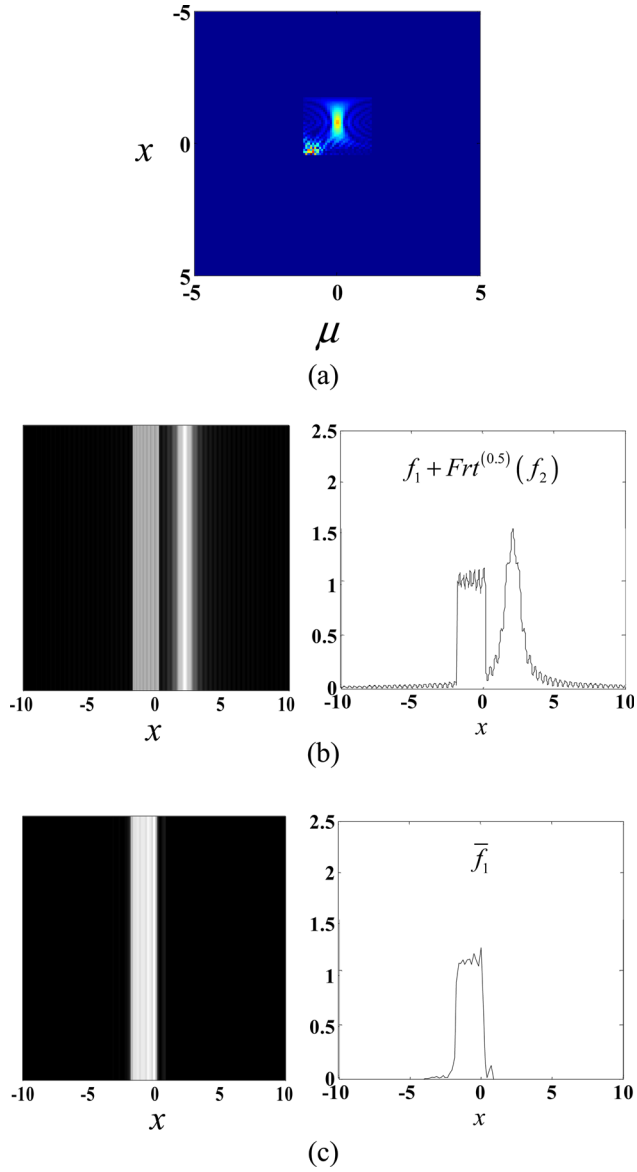

Fig. 6. (Color online) WDF filtering and signal reconstruction: (a) filtered WDF W_1 of $W_{f_1+f_{2,-a}}(x,\mu)$, (b) $s_{z_1}(x)$ and its line trace along x, (c) filtered signal $\bar{f}_1$ and its line trace along x.

left-hand side has been reconstructed without the defocus noise from the slit from the right-hand side on the reconstruction plane at $z = z_1$. We can also observe that, for the two-slit object without spatial overlapping, the simple binary filtering in the phase-space domain leads to successful optical sectioning within the OSH framework. When the reconstruction image plane is focused on $z = z_2$, the filtering is performed in the same manner. The filtered WDF, W_2, of $W_{f_{1,-a}+f_2}(x,\mu)$ obtained by a binary filter is shown in Fig. 7(a). In Figs. 7(b) and 7(c), the unfiltered reconstructed signal $s_{z_2}(x)$ and the filtered reconstructed signal $\bar{f}_2(x)$ are presented, respectively. Again, we can confirm that the defocused noise on the focused image plane is alleviated successfully even by the simple binary filtering in the phase-space domain, as is evident from Fig. 7(c), where the slit on the right-hand side has been reconstructed without the defocus noise from the slit from the left-hand side.

B. Optical Sectioning of Two-Slit Object with Spatial Overlapping

Let us consider a more complicated case in which the two slits are partially overlapped. Figure 8(a) shows sectional signals $f_1(x)$ and $f_2(x)$ and their relative positions in a 3-D Cartesian coordinate system.

Let us assume that the complex hologram takes the form of Eq. (23). In Fig. 8(b), the amplitude profile of the synthesized OSH complex hologram is presented. Within this setup, the reconstructed sectional signals without optical sectioning processing

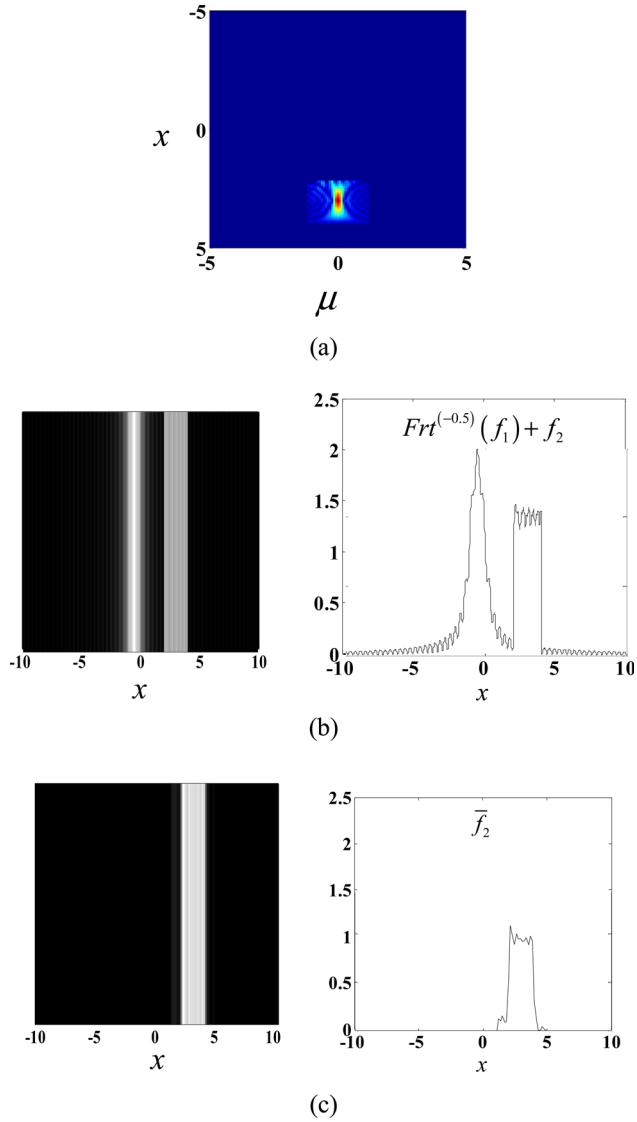

Fig. 7. (Color online) WDF filtering and signal reconstruction: (a) filtered WDF W_2 of $W_{f_{1,-a}+f_2}(x,\mu)$, (b) $s_{z_2}(x)$ and its line trace along x, (c) filtered signal $\bar{f}_2$ and its line trace along x

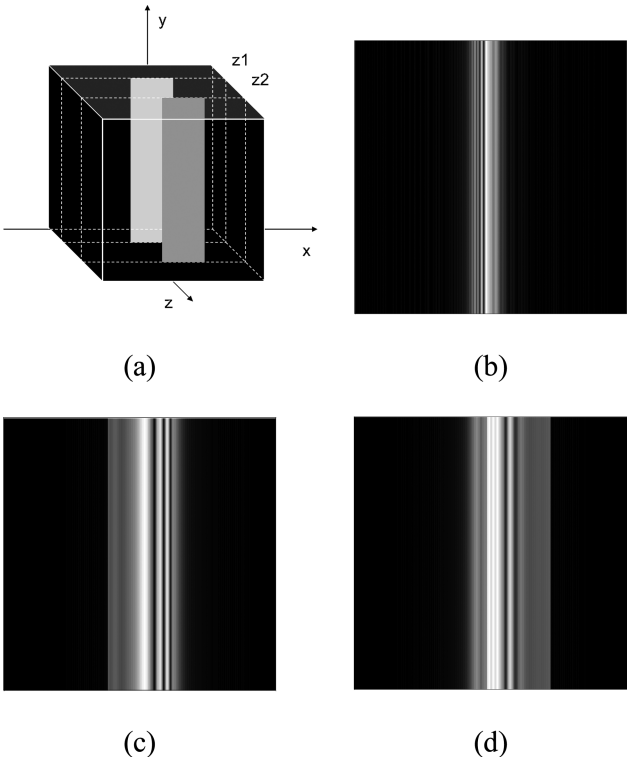

Fig. 8. (a) Two slits, (b) amplitude profile of the complex hologram $\varphi(x)$ given by Eq. (23), (c) $s_{z_1}(x)$ given by Eq. (24a), (d) $s_{z_2}(x)$ given by Eq. (24b).

are given by the forms of Eqs. (24a) and (24b). The reconstructed sectional signals $s_{z_1}(x)$ and $s_{z_2}(x)$ are shown in Figs. 8(c) and 8(d), respectively. As is seen in Figs. 8(c) and 8(d), the reconstructed signals include the focused signal, the defocused signal, and the interference pattern of two signals in the overlapping region. In Fig. 8(c), the left-hand slit is in focus, whereas the right-hand slit is defocused. In Fig. 8(d), the right-hand slit is in focus and the left-hand slit is out of focus.

The results of $W_{f_1+f_{2,a}}(x,\mu)$ and $W_{f_{1,-a}+f_2}(x,\mu)$ are illustrated, respectively, in Figs. 9 and 10 for $a = 0.5$. The three partial terms comprising the WDF, which are related to the focused signal, the defocused signal, and the interference term, are separately shown to aid in understanding the filtering principle.

In the same manner as in the previous nonoverlapping example, filtering is performed to eliminate the parts of the defocused signal and the cross term. However, we should use a more refined filter structure than that used for the previous example without spatial overlapping. Before devising the filter, let us consider the signal structure of the WDF of two-slit signals. We basically assume that signals are low bandwidth, which means the WDF of the focused signal is concentrated around the space axis (x axis) as shown in Figs. 9(b) and 10(c).

The principle of the WDF filtering is illustrated in Fig. 11. For comparison, the WDF filterings of $W_{f_1+f_{2,-a}}(x,\mu)$ and $W_{f_{1,-a}+f_2}(x,\mu)$ are shown in

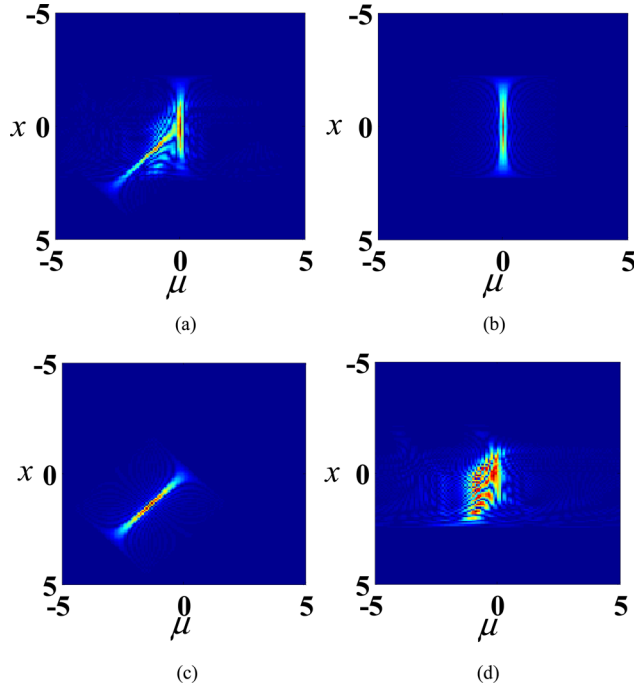

Fig. 9. (Color online) (a) WDF of $s_{z_1}(x)$: $W_{f_1+f_{2,a}}(x,\mu)$, (b) $W_{f_1}(x,\mu)$, (c) $W_{f_{2,a}}(x,\mu)$, (d) $C_{f_1+f_{2,a}}(x,\mu)$.

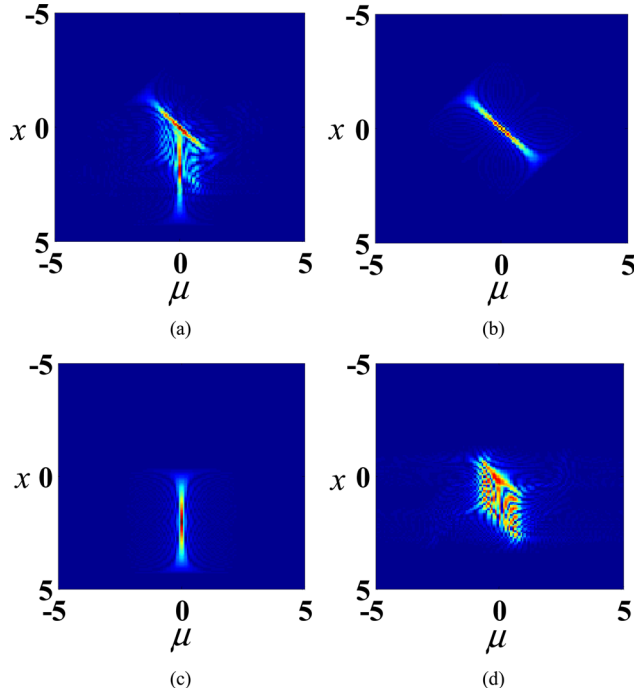

Fig. 10. (Color online) (a) WDF of $s_{z_2}(x)$: $W_{f_{1,-a}+f_2}(x,\mu)$, (b) $W_{f_{1,-a}}(x,\mu)$, (c) $W_{f_2}(x,\mu)$, (d) $C_{f_{1,-a}+f_2}(x,\mu)$.

Figs. 11(a) and 11(b), respectively. The three composite terms of the WDF, the WDF of a focused signal, the WDF of a defocused signal, and the cross term are simply drawn in the part indicated by the term 'WDF' in Figs. 11(a) and 11(b), respectively.

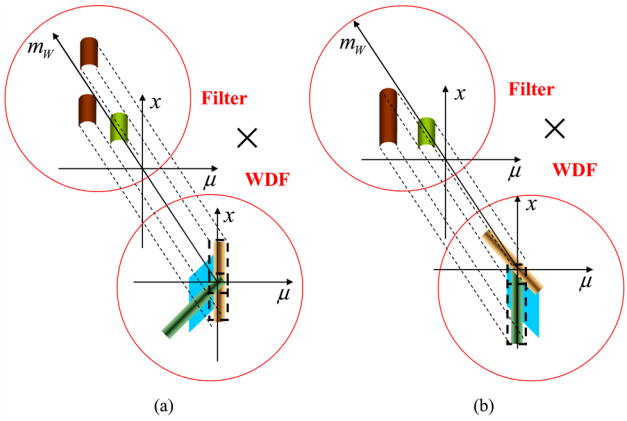

Fig. 11. (Color online) Concept of WDF filtering: filtering of (a) $W_{f_1+f_{2,-a}}(x,\mu)$ and (b) $W_{f_{1,-a}+f_2}(x,\mu)$.

The most useful property of the WDF in the phase-space domain is that the defocused signal is separated by the geometric rotation. We can eliminate the part outside the rectangular dashed lines while keeping everything inside the rectangular dashed lines as indicated in Figs. 11(a) and 11(b). By simple binary filtering, most of the rotated WDF of the defocused signal and the cross term with relatively wide frequency bandwidth can be rejected. This is the filtering used in the previous example when the two slits are spatially separated. In the case of partial overlap of the two slits, the different WDFs share the rotation center region. As a result, the WDF around the center has the larger values, the sum of the three terms. Hence it is necessary to damp the WDF around the cross area around the center. Thus the filter has a stepwise structure to apply different weights to the cross area around the center and the other areas of the WDF. Therefore the filter is designed to have a Gaussian window profile along the frequency axis (μ axis). The filter structures with these three elements for $W_{f_1+f_{2,-a}}(x,\mu)$ and $W_{f_{1,-a}+f_2}(x,\mu)$ are represented in the $x-\mu-m_W$ coordinate system (filter plane) in the parts indicated by the term 'Filter' in Figs. 11(a) and 11(b), respectively. The m_W axis denotes the magnitude of the filter weight. For example, the top part of the dashed rectangular area has the largest weight as shown in Fig. 11. Hence, the three truncated Gaussian windows are multiplied by the WDFs to produce the filtered WDFs. This operation is represented by the 3-D projection of the filter structure in the 'Filter' part to the 'WDF' plane. We can effectively remove the cross term and the defocused term from the WDF in phase space by means of the devised filter structure in the phase-space domain.

In Figs. 12 and 13, the WDF filtering and signal reconstruction of $f_1(x)$ from $s_{z_1}(x)$ and those of $f_1(x)$ from $s_{z_1}(x)$ are illustrated, respectively. The filter structure composed of three truncated Gaussian windows and the filtered WDF of $W_{f_1+f_{2,a}}(x,\mu)$

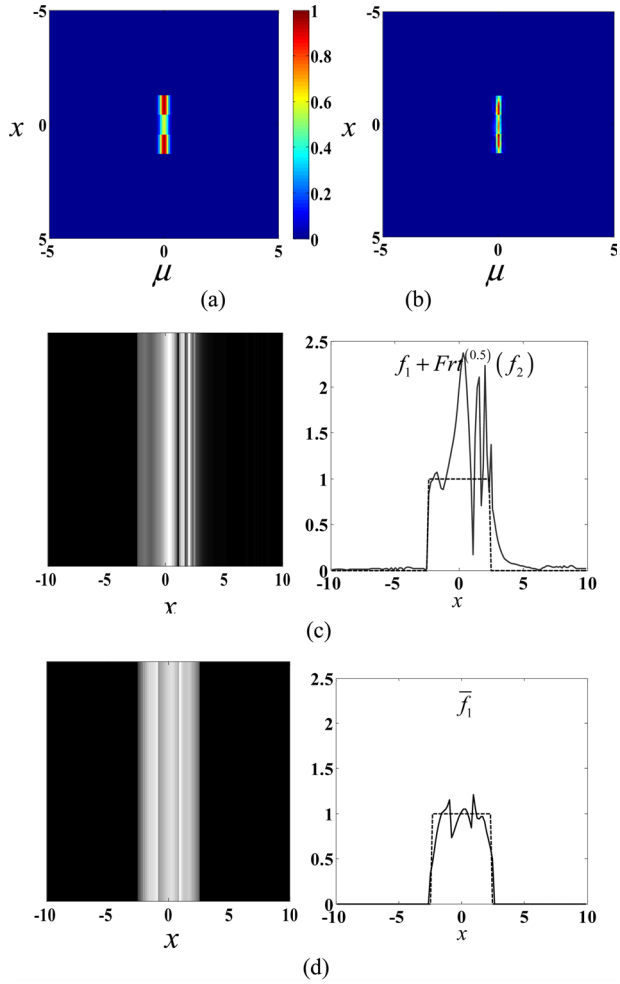

Fig. 12. (Color online) WDF filtering and signal reconstruction: (a) filter structure, (b) filtered WDF W_1 of $W_{f_1+f_{2,-a}}(x,\mu)$, (c) $s_{z_1}(x)$ and its line trace along x, (d) filtered signal $\bar{f}_1$ and its line trace along x.

obtained by the filter are shown in Figs. 12(a) and 12(b), respectively. In Figs. 12(c) and 12(d), the unfiltered reconstructed signal $s_{z_1}(x)$ and the filtered reconstructed signal $\bar{f}_1(x)$ are presented, respectively. We can see that the devised filtering in the phase space leads to successful optical sectioning within the OSH framework. When the focus is on $z=z_2$, the filtering is performed in the same manner. The filter structure and filtered WDF of $W_{f_{1,-a}+f_2}(x,\mu)$ obtained by the filter are shown in Figs. 13(a) and 13(b), respectively. In Figs. 13(d) and 13(c), the unfiltered reconstructed signal $s_{z_2}(x)$ and the filtered reconstructed signal $\bar{f}_2(x)$ are presented, respectively. The defocused noise on the focused image plane is alleviated successfully by the proposed filtering in the phase space.

4. Optical Sectioning of Two-Dimensional Signals

In this section, the phase-space optical sectioning method is extended to 2-D signals. In general, the

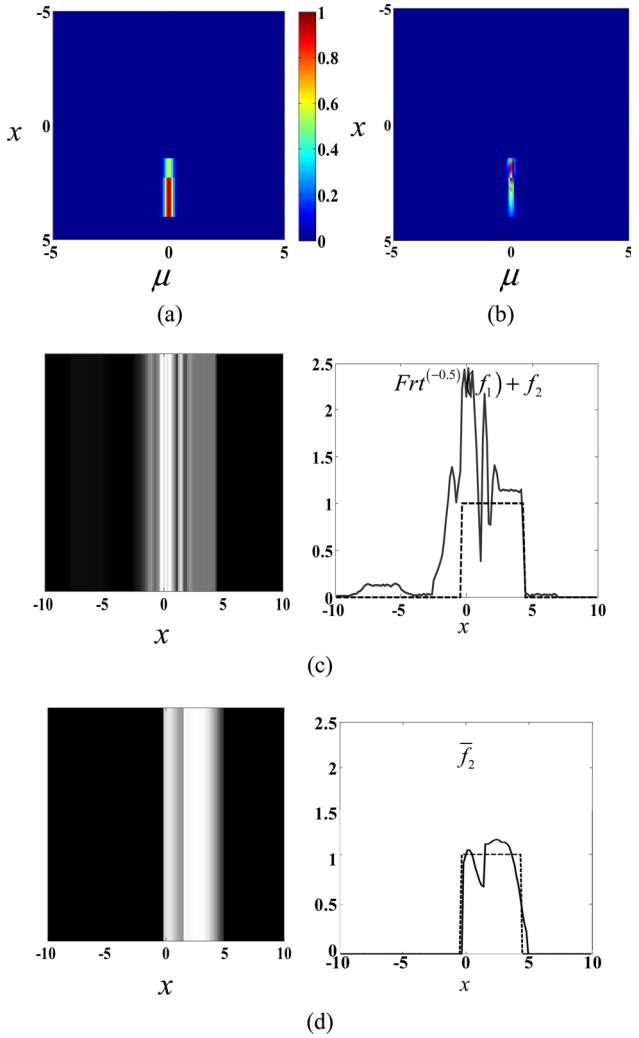

Fig. 13. (Color online) WDF filtering and signal reconstruction: (a) filter structure, (b) filtered WDF W_2 of $W_{f_{1-a}+f_2}(x,\mu)$, (c) $s_{z_2}(x)$ and its line trace along x (d) filtered signal $\bar{f}_2$ and its line trace along x.

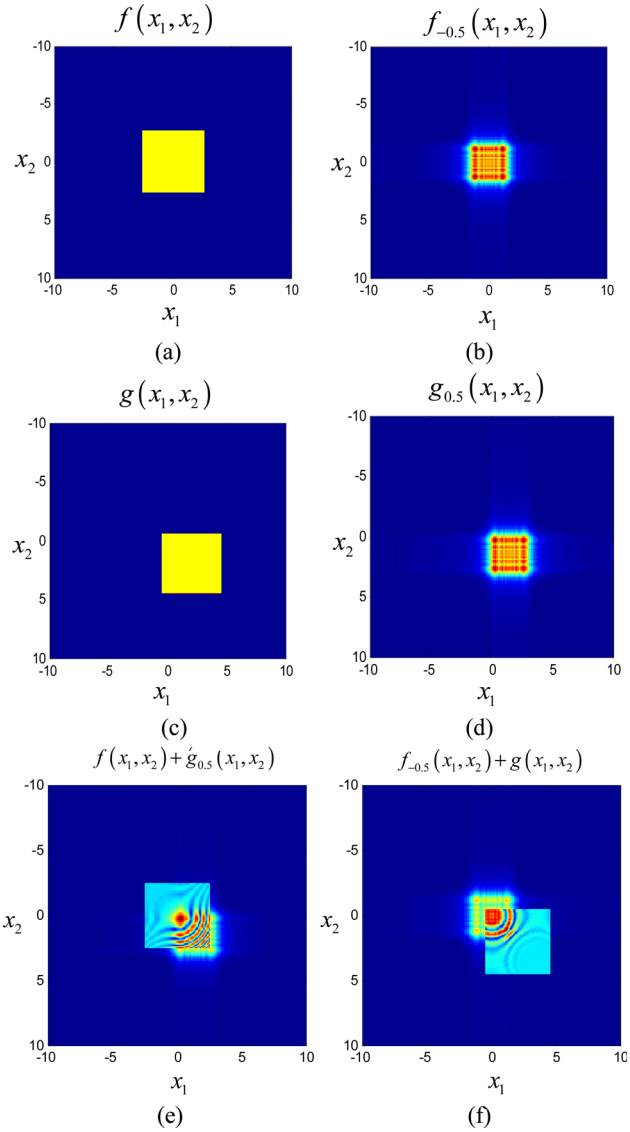

Fig. 14. (Color online) Example 2-D signals: (a) $f(x_1,x_2)$, (b) $f_{-0.5}(x_1,x_2)$, (c) $g(x_1,x_2)$, (d) $g_{0.5}(x_1,x_2)$, (e) $f(x_1,x_2)+g_{0.5}(x_1,x_2)$, (f) $f_{-0.5}(x_1,x_2)+g(x_1,x_2)$.

WDF of 2-D signal is a 4-D distribution. Although filtering of general 4-D Wigner signals should be further investigated in the aspects of algorithm and computation, in this paper we present the feasibility of the WDF filtering for optical sectioning of 2-D signals. Here we examine rectangular aperture signals $f(x_1,x_2)$ and $g(x_1,x_2)$ given, respectively, by

$$f(x_1,x_2)=f_1(x_1)f_2(x_2), \tag{26a}$$

$$g(x_1,x_2)=g_1(x_1)g_2(x_2), \tag{26b}$$

which are separable signals shown in Figs. 14(a) and 14(c), respectively. For convenience, $g(x_1,x_2)$ is simply the shifted version of $f(x_1,x_2)$. The ath-order 2-D FRFTs of $f(x_1,x_2)$ and $g(x_1,x_2)$ are also separable signals, as seen in Eq. (9). In Figs. 14(a) and 14(b), the signal $f(x_1,x_2)$ and its −0.5-order FRFT $f_{-0.5}(x_1,x_2)$ are shown, respectively. In Figs. 14(c) and 14(d), $g(x_1,x_2)$ and its 0.5-order FRFT $g_{0.5}(x_1,x_2)$ are shown, respectively. The reconstructed sectional signals without optical sectioning processing, $f(x_1,x_2)+g_{0.5}(x_1,x_2)$ and $f_{-0.5}(x_1,x_2)+g(x_1,x_2)$ are presented in Figs. 14(e) and 14(f), respectively. In the 2-D signal example, spatial-overlapping exists between $f(x_1,x_2)$ and $g(x_1,x_2)$ as in the previous 1-D signal example.

For the sectioning, first the WDF of the mixed signal is inspected. The WDFs of the sums of $f(x_1,x_2)$

and $g_a(x_1,x_2)$ and of $f_a(x_1,x_2)$ and $g(x_1,x_2)$ are given, respectively, by

$$\begin{aligned}W_{f+g_a}(x_1,x_2,\mu_1,\mu_2) &= \iint [f(x_1+x_1'/2,x_2+x_2'/2)+g_a(x_1+x_1'/2,x_2+x_2'/2)][f^*(x_1+x_1'/2,x_2+x_2'/2)\\ &\quad + g_a^*(x_1+x_1'/2,x_2+x_2'/2)]\mathrm{d}x_1'\mathrm{d}x_2'\\ &= W_{f_1}(x_1,\mu_1)W_{f_2}(x_2,\mu_2)+C_{f_1,g_{1,a}^*}(x_1,\mu_1)C_{f_2,g_{2,a}^*}(x_2,\mu_2)+C_{g_{1,a},f_1^*}(x_1,\mu_1)C_{g_{2,a},f_2^*}(x_2,\mu_2)\\ &\quad + W_{g_{1,a}}(x_1,\mu_1)W_{g_{2,a}}(x_2,\mu_2),\end{aligned} \tag{27a}$$

$$\begin{aligned}W_{f_a+g}(x_1,x_2,\mu_1,\mu_2) &= \iint [f_a(x_1+x_1'/2,x_2+x_2'/2)+g(x_1+x_1'/2,x_2+x_2'/2)][f_a^*(x_1+x_1'/2,x_2+x_2'/2)\\ &\quad + g^*(x_1+x_1'/2,x_2+x_2'/2)]\mathrm{d}x_1'\mathrm{d}x_2'\\ &= W_{f_{1,a}}(x_1,\mu_1)W_{f_{2,a}}(x_2,\mu_2)+C_{f_{1,a},g_1^*}(x_1,\mu_1)C_{f_{2,a},g_2^*}(x_2,\mu_2)+C_{g_1,f_{1,a}^*}(x_1,\mu_1)C_{g_2,f_{2,a}^*}(x_2,\mu_2)\\ &\quad + W_{g_1}(x_1,\mu_1)W_{g_2}(x_2,\mu_2).\end{aligned} \tag{27b}$$

Similar to the situation in the 1-D case as shown in Eqs. (24a) and (24b), we set $a=0.5$ in Eq. (27a) and $a=-0.5$ in Eq. (27b) for simulations.

It is noted that the WDF of the sum of two separable signals is not separable. However, in this example, the separability of the signals can be exploited for the filtering. Considering Eqs. (27a) and (27b), we can see that the separated parts, $f_1(x_1)$ and $f_2(x_2)$, of the signal $f(x_1,x_2)$ can be reconstructed in the 2-D phase space, not in the 4-D phase space.

The filtering process for the separable 2-D signal is as follows. First, with x_2 and μ_2 fixed, the WDF W_1 of $f(x_1,x_2)+g_a(x_1,x_2)$ is calculated:

$$\begin{aligned}W_1 &= W_{f+g_a}(x_1,x_2,\mu_1,\mu_2)\\ &= a_1W_{f_1}(x_1,\mu_1)+b_1W_{g_{1,a}}(x_1,\mu_1)\\ &\quad + 2\,\mathrm{Re}[c_1C_{f_1,g_{1,a}^*}(x_1,\mu_1)].\end{aligned} \tag{28}$$

In this example with the FRFT order parameter $a=0.5$, x_2 and μ_2 are set to 0. The values of x_2 and μ_2 are selected to maximize the ratios of a_1/b_1 and a_1/c_1. This operation damps the undesired terms effectively. In this example, for $x_2=0$ and $\mu_2=0$, a_1, b_1, and c_1 are obtained, respectively, by $a_1=W_{f_2}(0,0)=10$, $b_1=W_{g_{2,0.5}}(0,0)=2$, and $c_1=C_{f_2,g_{2,0.5}^*}(0,0)=2$. In the same manner, we can calculate the WDF W_2 of $f(x_1,x_2)+g_a(x_1,x_2)$ with x_1 and μ_1 set to 0.

The calculation results for W_1 and W_2 are shown in Figs. 15(a) and 15(b), respectively. We can reconstruct the filtered 1D signals $\tilde{f}_1(x_1)$ and $\tilde{f}_2(x_2)$ by using the 1-D signal filtering procedure described in Section 3.

Finally, the reconstructed 2-D signal $\tilde{f}(x_1,x_2)=\tilde{f}_1(x_1)\tilde{f}_2(x_2)$ is obtained. In the same manner, $\tilde{g}(x_1,x_2)=\tilde{g}_1(x_1)\tilde{g}_2(x_2)$ can be calculated. The filtering results are presented in Fig. 16. In Figs. 16(a) and 16(b), the unfiltered reconstructed $f(x_1,x_2)+g_{0.5}(x_1,x_2)$ and the filtered signal $\tilde{f}(x_1,x_2)=\tilde{f}_1(x_1)\tilde{f}_2(x_2)$ are presented, respectively. In Figs. 16(c) and 16(d), the unfiltered reconstructed $f_{-0.5}(x_1,x_2)+g(x_1,x_2)$ and the filtered signal $\tilde{g}(x_1,x_2)=\tilde{g}_1(x_1)\tilde{g}_2(x_2)$ are presented, respectively.

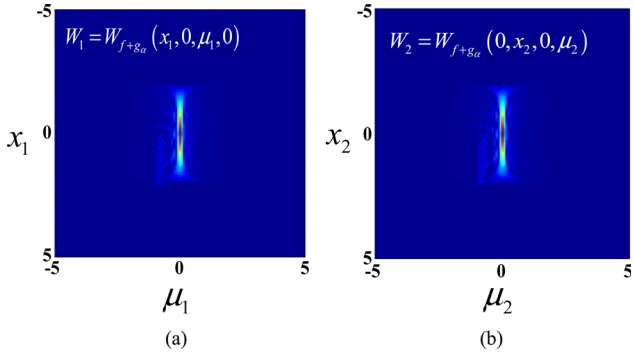

Fig. 15. (Color online) WDFs of $f(x_1,x_2)+g_{0.5}(x_1,x_2)$ at specific phase-space points (a) $(x_2,\mu_2)=(0,0)$ and (b) $(x_1,\mu_1)=(0,0)$.

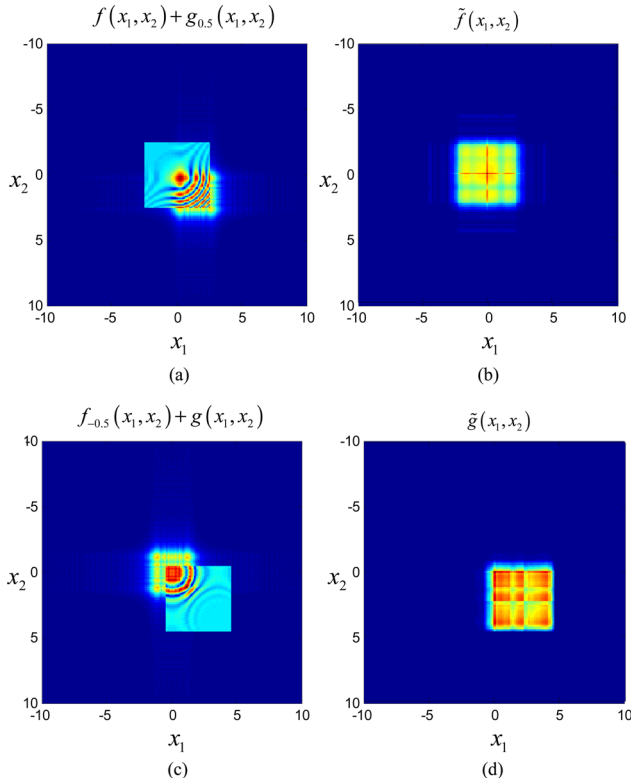

Fig. 16. (Color online) (a) Unfiltered sectional signal $f(x_1,x_2)+g_{0.5}(x_1,x_2)$ and (b) filtered sectional signal $\tilde{f}(x_1,x_2)$. (c) Unfiltered sectional signal $f_{-0.5}(x_1,x_2)+g(x_1,x_2)$ and (d) filtered sectional signal $\tilde{g}(x_1,x_2)$.

This example of 2-D signal sectioning shows that it is feasible for the defocused noise on the focused image plane to be alleviated successfully even by the filtering in the phase space.

5. Concluding Remarks

We have proposed a novel optical sectioning method using phase-space filtering with the introduction of the fractional Fourier transform to represent defocused information. The proposed technique is useful for a complex Fresnel zone plate hologram obtained by optical scanning holography, as the complex hologram does not contain any twin-image information. Simulations have been performed to demonstrate optical sectioning successfully with 1-D slit-type objects and 2-D rectangular-type objects. The proposed concept of phase-space filtering could possibly be extended and applied to more general 2-D images with some refinement in terms of computational complexities. In our results on 2-D objects, however, we have found that the proposed technique can even somewhat resolve occlusion, which means that the sectional image can be reconstructed even though the objects overlap.

This work was supported by a Korea Research Foundation grant funded by the Korean government (Ministry of Education and Human Resources Development, KRF-2005-214-D00290)

References

1. H. J. Caulfield, "Automated analysis of particle holograms," Opt. Eng. **24**, 462–463 (1985).
2. C. S. Vikram and M. L. Billet, "Far-field holography at non-image planes for size analysis of small particles," Appl. Phys. B **33**, 149–153 (1984).
3. D. A. Agard, "Optical sectioning microscopy: celluar architecture in three dimensions," Annu. Rev. Biophys. Bioeng. **13**, 191–219 (1984).
4. K. R. Castleman, *Digital Image Processing* (Prentice-Hall, 1979).
5. E. N. Leith, W.-C. Chein, K. D. Mils, B. D. Athey, and D. S. Dilworth, "Optical sectioning by holographic coherence imaging: a generalized analysis," J. Opt. Soc. Am. A **20**, 380–387 (2003).
6. T. Kim, "Optical sectioning by optical scanning holography and a Wiener filter," Appl. Opt. **45**, 872–879 (2006).
7. T.-C. Poon, "Scanning holography and two-dimensional image processing by acousto-optic two-pupil synthesis," J. Opt. Soc. Am. A **2**, 521–527 (1985).
8. T.-C. Poon, K. Doh, B. Schilling, M. Wu, K. Shinoda, and Y. Suzuki, "Three-dimensional microscopy by optical scanning holography," Opt. Eng. **34**, 1338–1344 (1995).
9. T.-C. Poon and T. Kim, "Optical image recognition of three-dimensional objects," Appl. Opt. **38**, 370–381 (1999).
10. T.-C. Poon, *Optical Scanning Holography with MATLAB* (Springer, 2007).
11. T.-C. Poon and T. Kim, *Engineering Optics with MATLAB* (World Scientific, 2006).
12. D. Dragoman, "*The Wigner distribution function in optics and optoelectronics*," in *Progress in Optics*, E. Wolf, ed. (Elsevier, 1997), Vol. 37, pp. 1–56.
13. H. M. Ozaktas, Z Zalevsky, and M. A. Kutay, *The Fractional Fourier Transform with Applications in Optics and Signal Processing* (Wiley, 2001).
14. R. F. O'Connell, "The Wigner distribution function—50th birthday," Found. Phys. **13**, 83–92 (1983).
15. J. Hahn, H. Kim, and B. Lee, "Optical implementation of iterative fractional Fourier transform algorithm," Opt. Express **14**, 11103–11104 (2006).
16. J. W. Goodman, *Introduction to Fourier Optics*, 3rd ed. (Roberts & Company, 2004).
17. H. Kim, B. Yang, and B. Lee, "Iterative Fourier transform algorithm with regularization for the optimal design of diffractive optical elements," J. Opt. Soc. Am. A **21**, 2353–2365 (2004).